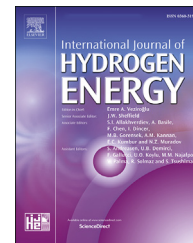




ELSEVIER

Available online at [www.sciencedirect.com](http://www.sciencedirect.com)

ScienceDirect

journal homepage: [www.elsevier.com/locate/he](http://www.elsevier.com/locate/he)

# Atomistic origin of mechanochemical $\text{NH}_3$ synthesis on Fe catalysts

Hong Woo Lee<sup>1</sup>, Ga-Un Jeong<sup>1</sup>, Min-Cheol Kim, Donghun Kim<sup>\*\*\*</sup>,  
Sooyeon Kim<sup>\*\*</sup>, Sang Soo Han<sup>\*</sup>

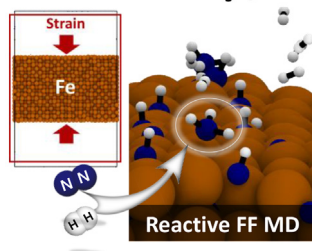
Computational Science Research Center, Korea Institute of Science and Technology, Seoul 02792, Republic of Korea

## HIGHLIGHTS

- Mechanochemical  $\text{NH}_3$  synthesis using ball-milling method is modeled by reactive molecular dynamics.
- Strain applied to Fe(110) significantly enhances the  $\text{N}_2$  dissociation as well as the  $\text{NH}_x$  ( $x = 1-3$ ) formation.
- From the von Mises stress analyses, applied strain transfers energy to Fe and \*N and then activates  $\text{NH}_3$  formation.
- New NH formation mechanism is proposed as a dominant process by DFT calculations.

## GRAPHICAL ABSTRACT

### Mechanochemical $\text{NH}_3$ synthesis



## ARTICLE INFO

### Article history:

Received 8 July 2022

Received in revised form

15 October 2022

Accepted 22 October 2022

Available online 17 November 2022

### Keywords:

$\text{NH}_3$  synthesis

Fe

Catalysts

Mechanochemical

ReaxFF

Molecular dynamics

\* Corresponding author.

\*\* Corresponding author.

\*\*\* Corresponding author.

E-mail addresses: [donghun@kist.re.kr](mailto:donghun@kist.re.kr) (D. Kim), [sooyeonk0806@kist.re.kr](mailto:sooyeonk0806@kist.re.kr) (S. Kim), [sangsoo@kist.re.kr](mailto:sangsoo@kist.re.kr) (S.S. Han).

<sup>1</sup> These authors contributed equally.

<https://doi.org/10.1016/j.ijhydene.2022.10.193>

0360-3199/© 2022 The Author(s). Published by Elsevier Ltd on behalf of Hydrogen Energy Publications LLC. This is an open access article under the CC BY-NC-ND license (<http://creativecommons.org/licenses/by-nc-nd/4.0/>).

## ABSTRACT

A tremendous amount of ammonia ( $\text{NH}_3$ ) has been produced by the Haber-Bosch method during the last 100 years. However, it is imperative to develop a new alternative to produce  $\text{NH}_3$  in a more environmentally friendly way due to the high energy cost and the large amount of greenhouse gas emissions in the Haber-Bosch method. Although the mechanochemical process has been regarded as an emerging technique, the understanding at the atomic level is limited. Here, we computationally model the mechanochemical ball-milling method by molecular dynamics simulations with the reactive force field (ReaxFF) developed in this work. We find that strain applied to Fe surfaces significantly enhances the  $\text{N}_2$  dissociation as well as the  $\text{NH}_x$  ( $x = 1-3$ ) formation on Fe(110), whereas the strain effect is negligible on Fe(111). From the von Mises stress analyses, the applied strain (mechanical) energies transfer to the Fe catalysts and N atoms adsorbed on Fe surfaces and then activate  $\text{NH}_x$  formation. Moreover, mechanical strain boosts a new mechanism for NH formation, the rate-determining step, via the direct interaction between the dissociated N atom on the Fe surface and the  $\text{H}_2$  molecule, which is supported by density functional theory

calculations. This study shows that the mechanochemical process is readily operated on Fe catalysts and promising for  $\text{NH}_3$  synthesis.

© 2022 The Author(s). Published by Elsevier Ltd on behalf of Hydrogen Energy Publications LLC. This is an open access article under the CC BY-NC-ND license (<http://creativecommons.org/licenses/by-nc-nd/4.0/>).

## Introduction

Ammonia ( $\text{NH}_3$ ) plays a key role in various industries, such as fertilizers [1–6] and nitrogen-containing chemicals [7]. Moreover, it has recently been in the spotlight as the best means of hydrogen carrier [8,9]. Despite various attempts over a century,  $\text{NH}_3$  is still produced mainly by the Haber-Bosch method. This process is not only extremely energy-intensive with a large amount of greenhouse gas emissions but also requires a high cost to operate the  $\text{NH}_3$  production facility due to the harsh operating conditions: high temperatures (400–500 °C) and pressures (150–300 bar) [10,11].

Very recently, Han et al. [12] reported a groundbreaking method for  $\text{NH}_3$  production based on mechanochemistry. Via an iron (Fe) ball-milling process consisting of two steps, nitrogen ( $\text{N}_2$ ) dissociation and subsequent hydrogenation, they achieved a superior  $\text{NH}_3$  concentration (82.5 vol%) under mild reaction conditions (45 °C and 1 bar), indicating a much higher  $\text{NH}_3$  production than the 25 vol% from the state-of-the-art Haber-Bosch method at 450 °C and 200 bar conditions [5,13,14]. Although the mechanochemical method is a two-step synthesis process, it definitely provides opportunities to save the amount of energy required to produce  $\text{NH}_3$  and is an eco-friendly (solvent-free), economically cheap and scalable manufacturing process [15]. The previously reported energy consumption values of the Haber-Bosch process are 36.4 (in 1970s) - 28.0 (in 2010s)  $\text{GJ}/\text{t}_{\text{NH}_3}$  based on the conventional methane-fed process, and 39.7 (in 1970s) - 38.4 (in 2010s)  $\text{GJ}/\text{t}_{\text{NH}_3}$  by the electric power [5]. On the other hands, Han et al. [12], reported that the energy consumption of the ball-milling process based on mechanochemical methods is 4.5  $\text{GJ}/\text{t}_{\text{NH}_3}$ , which is about 9 times more energy-saving process than the Haber-Bosch process.

It was reported that the rate-determining step for the mechanochemical synthesis of  $\text{NH}_3$  operated at low temperature is the hydrogenation process of  $\ast\text{N}$  ( $\ast$  denotes a surface site) dissociated on Fe surfaces because the Fe surfaces can be easily blocked from strongly adsorbed hydrogen atoms [12,16,17], which is in contrast to the Haber-Bosch process operated at high temperature, where the rate-determining step is  $\text{N}_2$  dissociation [13,18–20]. In the ball-milling process by Han et al. violent impacts facilitate the desorption of hydrogen-related intermediates on Fe catalysts and then can promote  $\text{NH}_3$  synthesis [12]. They also demonstrated a theoretical understanding of the  $\text{NH}_3$  synthesis mechanism of the mechanochemical process by density functional theory (DFT) calculations, in which they proposed a dynamic relaxation model to explain the effects of the violent impact inducing rearrangement of the lattice parameters and atom positions of Fe during a ball-milling process on  $\text{NH}_3$  synthesis. Undoubtedly, the theoretical approach provides a valuable explanation

to understand the mechanism of mechanochemical  $\text{NH}_3$  synthesis. However, due to the limit of DFT calculations, there remains room to explore the real dynamic behaviors of atoms involved in the mechanochemical process. Moreover, the dynamic relaxation model was investigated only for Fe(110) surfaces. Although the (110) surface is thermodynamically most favorable for Fe, the high collisions between Fe catalysts and balls during the ball-milling process would lead to the evolution of other surfaces, motivating us to investigate the effects of Fe surfaces on mechanochemical  $\text{NH}_3$  synthesis.

In this study, we use a molecular dynamics (MD) simulation with a reactive force field (ReaxFF) [21,22] to investigate the mechanochemical synthesis behaviors of  $\text{NH}_3$  on Fe catalysts at the atomic level. Because ReaxFF allows nanoscale systems with over 100,000 atoms [21,22], ReaxFF-MD simulations have played key roles in bridging experiments and theories in various fields, such as batteries [23,24], atomic layer depositions [25], combustions [26–29], biosystems [30], and catalysts [31–33]. In particular, we recently reported the activity, selectivity, and durability for  $\text{NH}_3$  synthesis on ruthenium (Ru) nanoparticle catalysts using ReaxFF-MD simulations [34]. Here, we first develop the ReaxFF parameters for the Fe–N–H system obtained from DFT calculations. Then, with the developed ReaxFF, mechanochemical  $\text{NH}_3$  synthesis on Fe catalysts is explored, where the mechanochemical process is modeled by two steps:  $\text{N}_2$  dissociation (formation of  $\ast\text{N}$ ) and hydrogenation (formation of  $\text{NH}_x$ , where  $x = 1–3$ ), as in the experiment [12]. We additionally investigate the effects of strain and Fe surface on mechanochemical  $\text{NH}_3$  synthesis and discuss a mechanism of impact-activated surface reactions on Fe catalysts, where the mechanism is confirmed with DFT calculations.

## Computational methods

To simulate  $\text{NH}_3$  generation from  $\text{N}_2$  and  $\text{H}_2$  gases on the Fe catalyst surfaces, we performed MD simulations with ReaxFF, in which the ReaxFF parameters for ternary Fe–N–H were required for the simulation. Based on the reported ReaxFF parameters for binary Fe–H [35] and N–H [34], we developed the force field parameters for the Fe–N–H system using DFT calculations. In particular, the bond parameters for Fe–N, the angle parameters for N–Fe–N and N–N–Fe, and the off-diagonal parameters for Fe–N were developed. The ReaxFF parameters were optimized from various DFT training data, where a successive one-parameter search technique [36] was used with one-dimensional parabolic extrapolation against the DFT data. We considered Fe–N, Fe– $\text{NH}_x$ , and  $\text{H}_2\text{N–Fe–NH}_2$  clusters in a nonperiodic system. For periodic systems, various reaction pathways for adsorption and diffusion of a N atom,  $\text{N}_2$  dissociation,  $\text{N}_2$  valence angle bending,  $\text{NH}_3$

desorption, and  $\text{NH}_3$  decomposition over the Fe surfaces were considered. The details on the ReaxFF development are available in the Supplementary data.

For DFT calculations of periodic systems, the Vienna Ab initio Simulation Package (VASP) [37] was used with an energy cutoff of 500 eV and the revised Perdew-Burke-Ernzerhof (rPBE) [38] exchange and correlation functional. A vacuum spacing of 15 Å was used to avoid interslab interactions. The project-augmented-wave method [39] was adopted to describe the core electrons, and Monkhorst-Pack k-point meshes of  $4 \times 4 \times 1$  were used for the slab calculations. While the bottom two layers in the Fe slabs were fixed, the top two layers and the reactant molecules were optimized until the energy change was less than  $1 \times 10^{-4}$  eV/cell and the force on each atom was less than  $0.02 \text{ eV \AA}^{-1}$ . In addition, the climbing-image nudged-elastic band (NEB) [40] method was employed to search the transition states (TSs) for hydrogenation reactions of the dissociated N (\*N) on Fe surfaces with 6 images.

Classical MD simulations were performed using the LAMMPS (Large-scale Atomic/Molecular Massively Parallel Simulator) software package [41,42] with the developed ReaxFF. We considered two low-index Fe surfaces: Fe(110), which is the most stable surface, and Fe(111), which is known to be the most activated surface for  $\text{NH}_3$  synthesis [43]. The Fe bulk was first energy-minimized by a conjugate algorithm and then relaxed using an isothermal-isobaric (NPT) ensemble at 1000 K and 1 atm. The Fe(110) and (111) slabs were cleaved from the optimized structure of a Fe bulk. The sizes of the slabs were  $56.6 \times 39.9 \times 36.4 \text{ \AA}$  for Fe(110) and  $56.5 \times 42.0 \times 34.6 \text{ \AA}$  for Fe(111) with a vacuum layer of 50 Å (along the z-axis) in a 3-dimensional periodic boundary cell. Prior to the introduction of reactant gas molecules into the simulation box, the slab structures were relaxed using a canonical (NVT) ensemble at 1000 K for 200 ps (picoseconds). Because the slab was thick enough (16–18 atomic layers), the atoms in the middle part of the slabs behaved as in the bulk. All reactions were carried out at 1000 K using a Nosé–Hoover thermostat in the NVT ensemble, in which the high reaction temperature was employed to accelerate the chemical reactions between solid catalysts and gas molecules [34,44]. The total MD simulation time was 1–1.5 ns (nanoseconds) with a time step of 0.25 fs (femtoseconds).

During MD simulations, the ammonia formation reaction was simulated in two steps, (1)  $\text{N}_2$  dissociation and (2) hydrogenation to form  $\text{NH}_x$  ( $x = 1-3$ ), to model the reported experiment [12]. This step-by-step method is useful to analyze factors that can affect the ammonia formation rate during the simulation. In the first step,  $\text{N}_2$  gases of 300 atm were purged into the simulation system and reacted with the Fe catalyst surfaces for 1 ns. In the second step, all surrounding  $\text{N}_2$  gases that did not participate in the surface reactions were removed. Then,  $\text{H}_2$  gases of 500 atm were added to the system. Prior to the ReaxFF-MD simulations for  $\text{NH}_3$  synthesis, to avoid the instability of the initial configurations of the reactant gases in the system, their initial positions were preoptimized by NVT-MD simulations at 1000 K with a nonreactive FF (universal force field) [45].

For each reaction step, several strains (0%, 3%, and 5%) were applied to the Fe catalysts to investigate the effect of strain on  $\text{NH}_3$  production. A constant strain was applied by

decreasing the cell size in the z-direction (perpendicular to the Fe surface) after 10,000 MD steps in which the Poisson ratio of Fe (0.29) [46] was considered. The deformation in the z-direction (compressive strain) was considered to model the impact of balls on the catalysts in the mechanochemical method, and the deformation was kept constant until the end of simulations. To investigate the correlation between the activity and mechanical deformation of the Fe catalyst surfaces, we also calculated the von Mises stress of each atom. The von Mises stress ( $\sigma_v$ ) eq. (1). is expressed as follows:

$$\sigma_v = \left\{ \frac{1}{2} \left[ (\sigma_{xx} - \sigma_{yy})^2 + (\sigma_{yy} - \sigma_{zz})^2 + (\sigma_{zz} - \sigma_{xx})^2 + 6(\sigma_{xy}^2 + \sigma_{yz}^2 + \sigma_{zx}^2) \right] \right\}^{1/2} \quad (1)$$

where  $\sigma_{xx}$ ,  $\sigma_{yy}$ , and  $\sigma_{zz}$  represent the normal stresses and  $\sigma_{xy}$ ,  $\sigma_{yz}$ ,  $\sigma_{zx}$  represent the shear stresses.

## Results and discussion

### $\text{N}_2$ dissociation

It is well known that the  $\text{N}_2$  dissociation reaction is the rate-limiting step of the Haber-Bosch process for  $\text{NH}_3$  synthesis [19,47–49]. However, in the mechanochemical method, the  $\text{N}_2$  dissociation process could be accelerated by comminution of Fe catalyst particles into smaller grains [12]. In addition to the generation of new grain surfaces, physical impact to the catalyst surfaces readily affects the  $\text{N}_2$  dissociation reaction because the high-speed ball-milling process can deform the surface structures. In this study, we modeled the ball-milling process by applying strain to Fe surfaces using ReaxFF-MD simulations (Fig. 1).

According to Bozso et al. [49,50], the ratio of initial rates for nitrogen adsorption on Fe surfaces at 550 K is (111):(100):(110) = 60:3:1. Here, because nitrogen adsorption is dissociative, it produces activated N atoms that can react with hydrogen to form ammonia. In regard to ammonia formation, the effects of the Fe surfaces become more prominent. Similarly, Spencer et al. found that the ratio of relative ammonia formation rates on Fe surfaces is (111):(100):(110) = 418:25:1 at 798 K [51]. These results reveal that Fe(111) is the most activated surface to produce ammonia, followed by Fe(100) and Fe(110). In addition, previous DFT calculations reported that the energy barrier for  $\text{N}_2$  dissociation on Fe(110) is 1.1–1.2 eV [52–54], which is similar to our DFT calculations. We obtained energy barriers of 0.56 eV, 1.15 eV, and 1.22 eV on Fe(111), Fe(100) and Fe(110), respectively. The ReaxFF developed in this work also showed the trend for  $\text{N}_2$  dissociation on Fe surfaces as Fe(111) > Fe(100) > Fe(110) (Fig. S10), similar to Bozso et al. [50].

Using ReaxFF-MD simulations, we applied a strain of 5% to the Fe(110) and Fe(111) catalyst surfaces and then measured the  $\text{N}_2$  dissociation rate and the formation of \*N (Fig. 1b–e), in which we observed a decrease in  $\text{N}_2$  and an increase in \*N with increasing MD time resulting from  $\text{N}_2$  dissociation and the \*N formation reaction, respectively. According to DFT calculations of Logadottir and Nørskov [52], a strained surface increases the nearest neighbor distance parallel to the surface by 1.3 Å, leading to a lower energy barrier by 0.38 eV on the

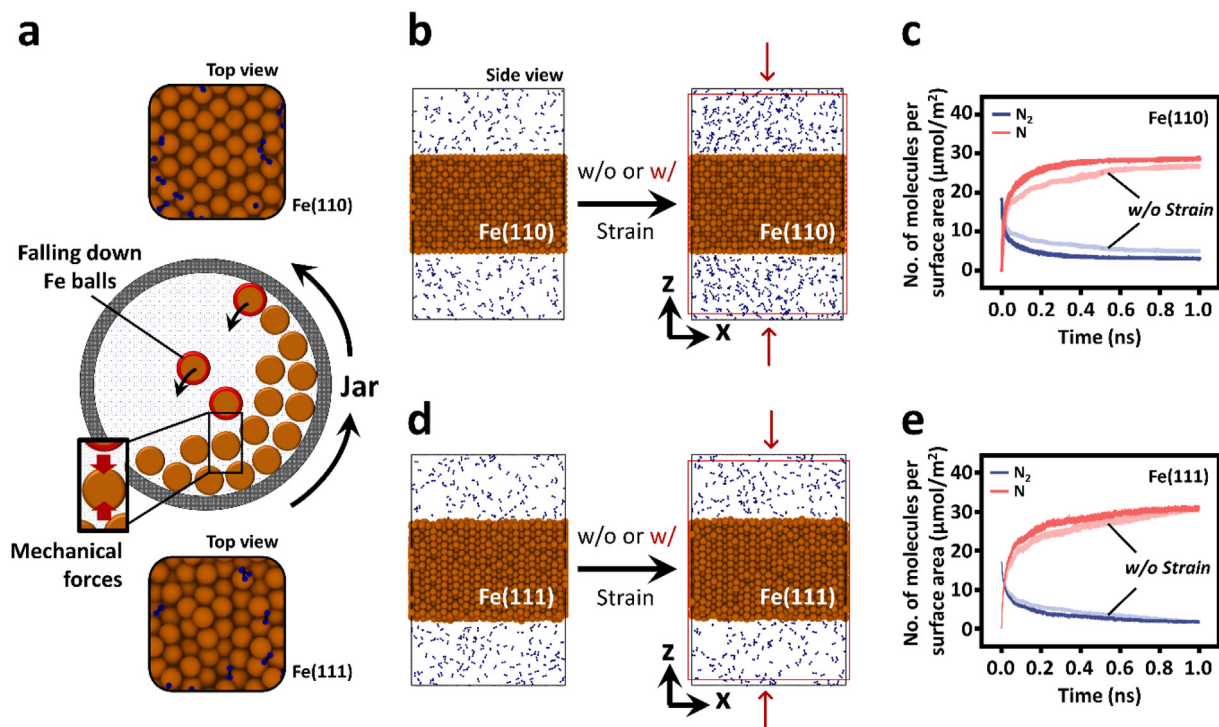


**Fig. 1** – Accelerated N<sub>2</sub> dissociation reaction using (a) a mechanochemical ball-milling process on (b,c) Fe(110), and (d,e) Fe(111). (c), (e) Red and blue lines indicate the numbers of N<sub>2</sub> molecules and dissociated N atoms, respectively. The lighter colored lines are for no applied strain, and the darker colored lines are when a strain of 5% along the z-axis is applied. Here, the color code for atoms is Fe = brown, and N = navy. (For interpretation of the references to color in this figure legend, the reader is referred to the Web version of this article.)

Fe(111) surface compared to the unstrained surface. When we apply a strain of 5%, the Fe surfaces show an increase in the initial reaction rates for N<sub>2</sub> dissociation (Fig. 1c and e). The exerted strain not only kinetically accelerates the N<sub>2</sub> dissociation reaction but also increases the amount of final product (\*N) by ~13% on Fe(110) and ~1% on Fe(111). Assuming the first-order reaction kinetics for N<sub>2</sub> dissociation, we calculated the rate constant *k* for the reaction. According to the first-order reaction kinetics,

$$\ln(N_t / N_0) = -kt \quad (2)$$

where *t* is the simulation time, *N<sub>t</sub>* is the number of N<sub>2</sub> molecules at time *t*, and *N<sub>0</sub>* is the number of N<sub>2</sub> molecules at time 0. The calculated reaction rate for 1 ns increases by 34% on Fe(110) and 4% on Fe(111), indicating that the strain effect is more pronounced on Fe(110) than Fe(111).

Considering the atomic distances on the Fe surfaces, the topmost layer of Fe(111) has longer distances between atoms than those of Fe(110). Thus, the deformation ratio of Fe(110) by the applied strain could be larger than that of Fe(111), leading to a more significant strain effect for N<sub>2</sub> dissociation on Fe(110). The radial distribution function (RDF) graphs in Fig. 2 show the average atomic distances of Fe atoms on the Fe(110) and Fe(111) surfaces in our MD simulations, where the atoms located within ~3 Å from the topmost surface are considered. The RDF analysis clearly supports the strain effect. While the distance between the nearest neighbors

(*r* ~ 2.5 Å) is increased by 2.4% for the Fe(110) surface, only 0.08% is increased for Fe(111). Although the strain effect on N<sub>2</sub> dissociation is more significant on Fe(110), a higher conversion is still observed on the Fe(111) surface. We observe more products (\*N) on the Fe(111) surface (90.2% of N<sub>2</sub> is reacted) than on the Fe(110) surface (82.7% of N<sub>2</sub> is reacted) after an MD simulation of 1 ns.

#### Hydrogenation to form ammonia

Hydrogenation of the N atoms adsorbed on the Fe catalyst surfaces is explored by analyzing the effect of physical impact on the hydrogenation step of NH<sub>3</sub> formation. The N-adsorbed Fe surface structures discussed in the previous section were used for these MD simulations, in which no strain condition was applied. Additionally, we deleted the residual N<sub>2</sub> gas molecules in the simulation box and added H<sub>2</sub> gas molecules of 500 atm. The details are described in the Computational Methods section. During the ReaxFF-MD simulations of 1.5 ns, the formation of NH<sub>3</sub> as well as the intermediates (\*NH and \*NH<sub>2</sub>) are observed in Fig. 3. Here, while the \*NH and \*NH<sub>2</sub> intermediates are adsorbed on the catalyst surface, many NH<sub>3</sub> products are desorbed from the Fe surfaces, which is supported by previous studies [55,56] comparing the adsorption energies of NH<sub>x</sub> (*x* = 1–3) species on the Fe(110) surface. NH<sub>3</sub> has adsorption energies of 0.62–0.83 eV on Fe(110) [55,56], which are much lower than those of NH or NH<sub>2</sub> intermediates (*E*<sub>ad, NH</sub> = –5.49 eV, *E*<sub>ad, NH<sub>2</sub></sub> = –3.17 eV) [56].

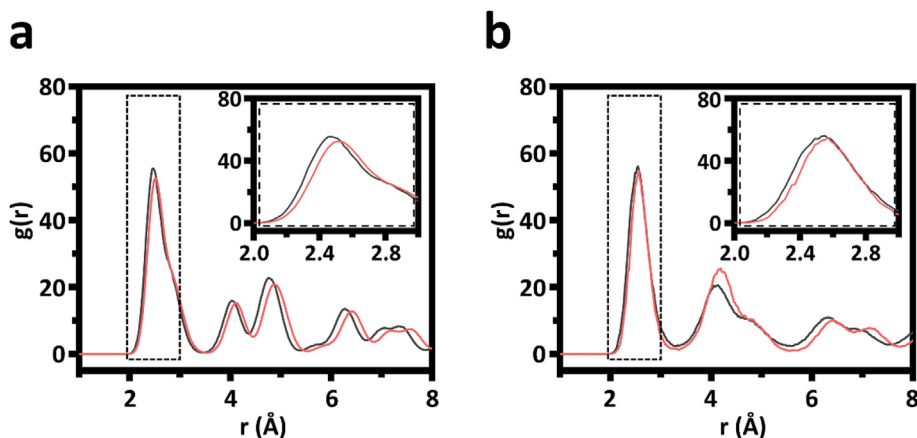


**Fig. 2** – RDFs of (a) Fe(110) and (b) Fe(111) surfaces before (black) and after 5% strain (red), calculated for  $\sim 3$  Å from the topmost surfaces. Insets are magnifications of the first peaks for each graph. (For interpretation of the references to color in this figure legend, the reader is referred to the Web version of this article.)

We also found that the strain effect on  $\text{NH}_3$  synthesis shows different behaviors for the Fe(110) and (111) surfaces. On the Fe(110) surface, as the degree of strain increases, the generated  $\text{NH}_3$  products and intermediates ( $\text{NH}_x$ ,  $x = 1-3$ ) increase (Fig. 3a–c). Up to 0.2 ns, the reaction rate for  $\text{NH}_x$  formation is approximately 2 times faster with 5% strain than that for the case with no strain. At 1.5 ns, the number of  $\text{NH}_x$  molecules produced is 77 and 112 when no strain and 5% strain are applied, respectively, where the formation of  $^*\text{NH}$  depends on the strain being more sensitive than those of  $^*\text{NH}_2$  and  $\text{NH}_3$ . The amount of  $\text{H}_2$  decreases over time because  $\text{H}_2$  is used for  $\text{NH}_x$  formation (Fig. 3d). In contrast, the strain effect is not significant on Fe(111) as much as on Fe(110) (Fig. 3e–h). In Fig. 2, we show that the  $\text{N}_2$  dissociation on Fe(111) is little affected by the strain. Accordingly, the strain does not significantly promote the hydrogenation process of the dissociated N atoms on the Fe(111) surface.

Under no strain, Fe(111) produces 32% more  $\text{NH}_x$  per surface area than Fe(110). On the Fe(110) surface, 72% of the reaction products are  $^*\text{NH}$ , and only 22% of them are  $^*\text{NH}_2$ , while  $^*\text{NH}$  of 58% and  $^*\text{NH}_2$  of 39% are produced on the Fe(111) surface. Because the hydrogenation energy barrier from  $^*\text{NH}$  to  $^*\text{NH}_2$  on Fe(111) is lower than those of other hydrogenation steps [57],  $^*\text{NH}$  can be relatively easily converted to  $^*\text{NH}_2$ . Compared to Fe(111), our MD simulation results show a lower conversion rate of  $^*\text{NH}$  to  $^*\text{NH}_2$  on the Fe(110) surface, which is likely because the energy barrier for the hydrogenation of  $^*\text{NH}$  to  $^*\text{NH}_2$  is much higher on Fe(110) [56]. On the other hand, under 5% strain, the total amounts of  $\text{NH}_x$  produced on Fe(110) and Fe(111) surfaces are similar after 1.5 ns ( $7.8 \mu\text{mol}/\text{m}^2$  for Fe(110) and  $7.2 \mu\text{mol}/\text{m}^2$  for Fe(111), Fig. S11), which is very noticeable because the strain can readily enhance catalytic performance for  $\text{NH}_3$  formation on Fe(110), although Fe(111) is more active for  $\text{NH}_3$  formation than on Fe(110) under no strain [51].

### Stress and energy analyses

To unveil the mechanism by which the physical impacts promote the formation of ammonia, we analyzed the local

energies and stresses of atoms during the MD simulations. First, we analyzed the system energy to confirm that the energy exerted by strain is indeed transferred to the atoms on the catalyst surface. When a strain of 5% is applied to the catalyst surface, a significant energy gain of the system is observed (Fig. S12), where after the energy gain, the system energy fluctuates slightly to relieve the exerted stress. Although the total energy of the system fluctuates, the average value is higher than before the strain is applied.

From the energy analyses of Fe, N, and H atoms in the system, the average atomic energies (sum of the potential and kinetic energies) of Fe and N increase upon applying strain (Fig. 4a and b), where all of the N atoms are adsorbed on the Fe surface. However, there is no significant energy gain for H atoms (Fig. 4c). These results clearly show that the energies generated by strain can increase the energies of the Fe catalyst and the species adsorbed on the surface so that the Fe catalyst and surface-adsorbed N can be readily further activated via the energy gain.

To further clarify the effects of the energies exerted by strain on the catalytic activity for  $\text{NH}_3$  synthesis, we performed von Mises stress analysis, in which the details on the calculation of the von Mises stress are described in the Computational Methods section. Fig. 4d and e shows the distribution of von Mises stresses of the Fe(110) and Fe(111) catalyst slabs before ( $t = 0$  s) and after applying 5% strain ( $t = 2.5$  ps) from our MD simulation results, where the map is normalized by the average von Mises stress of Fe for comparison between the two different faces: the actual stress ranges 0–27 GPa for Fe(110) and 0–31 GPa for Fe(111). Prior to application of the strain ( $t = 0$  s), higher surface stresses than the middle parts of the slabs are observed for both Fe(110) and Fe(111) due to the instability resulting from surface dangling bonds. Here, Fe(111) shows a higher surface stress than Fe(110), which is reasonable considering the surface reactivity of Fe(111). When strain is applied ( $t = 2.5$  ps), the stresses of both Fe surfaces increase overall. However, the change in the Fe(110) surface stress is much more noticeable, as already discussed.

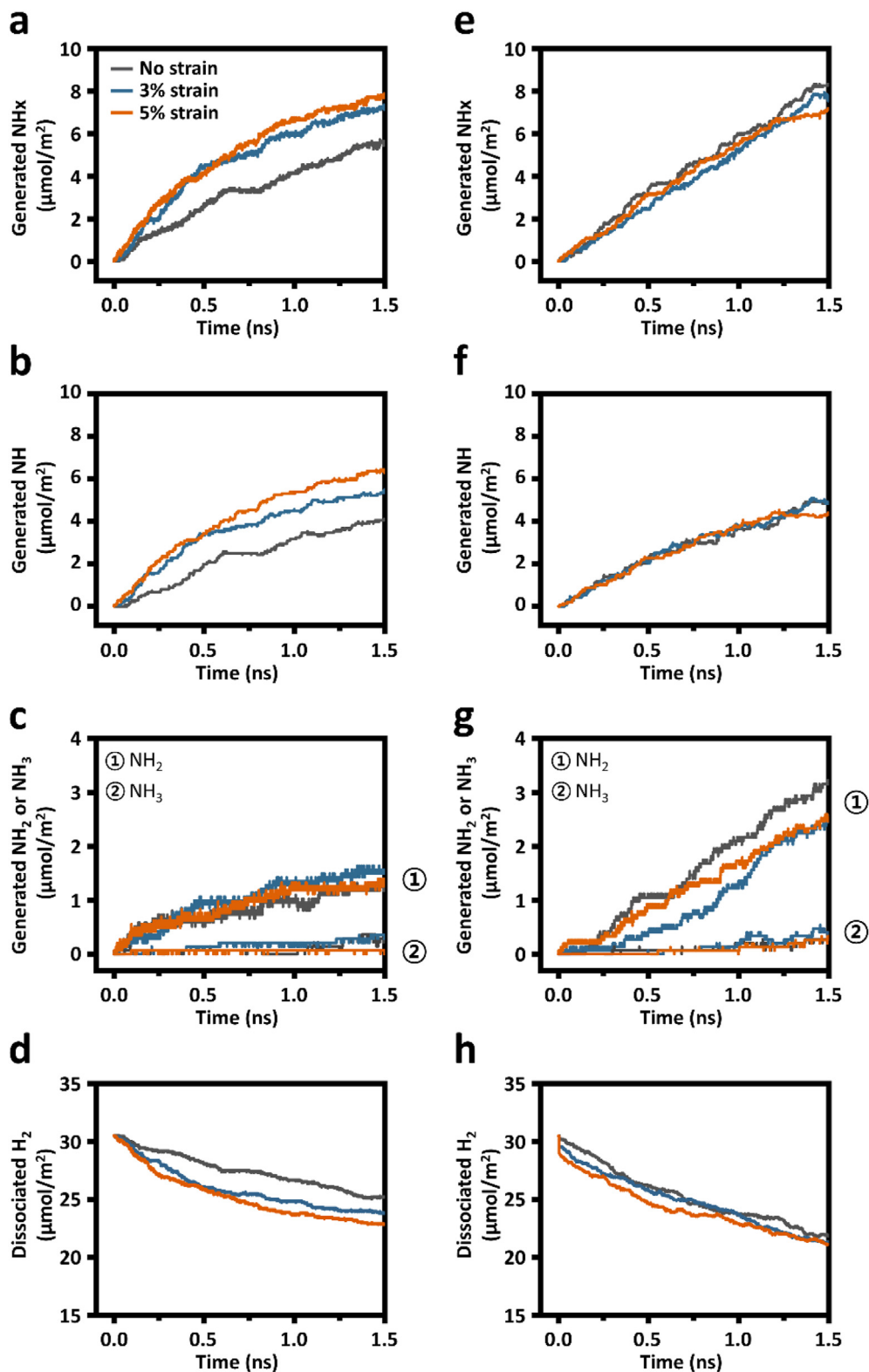
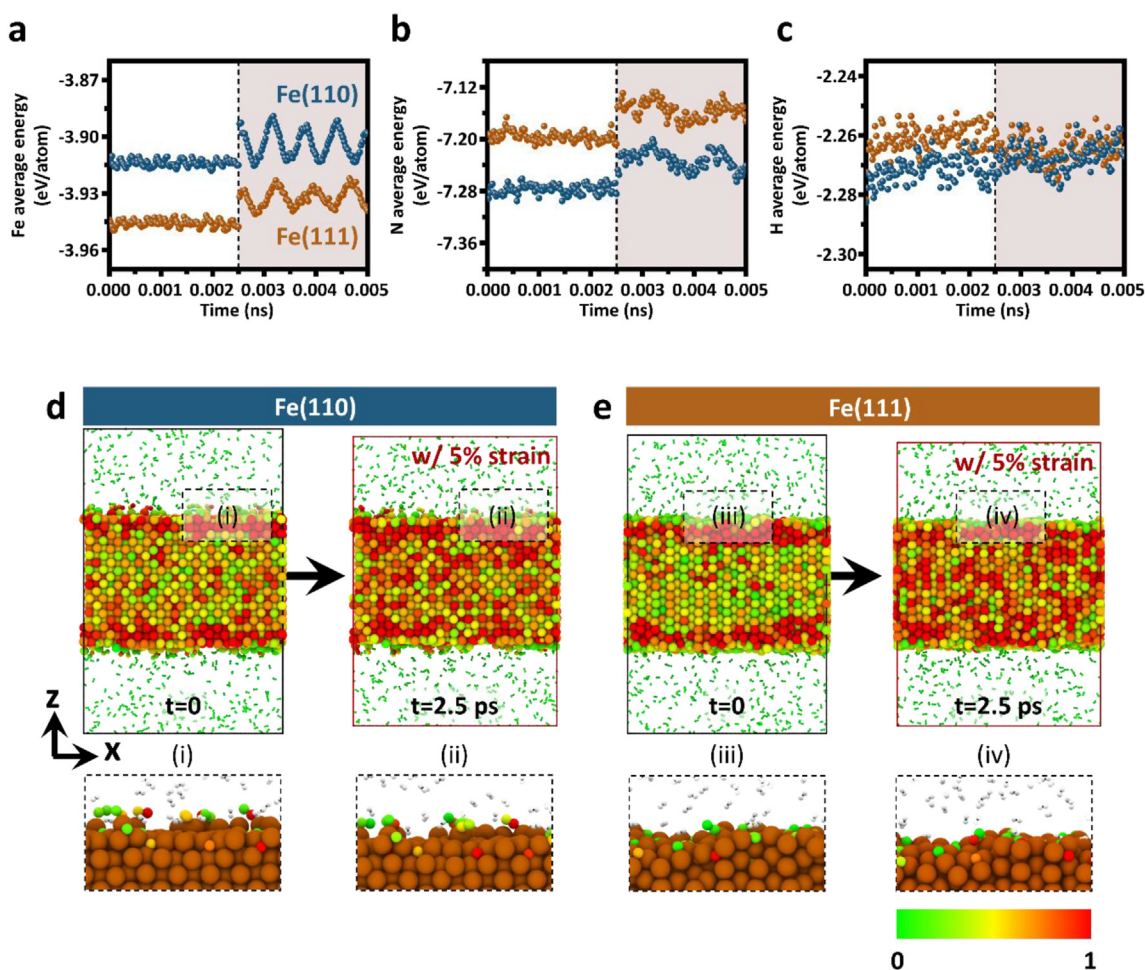


Fig. 3 – The amounts of  $\text{NH}_x$  ( $x = 1-3$ ) and  $\text{H}_2$  molecules generated or dissociated on the (a–d) Fe(110) and (e–h) Fe(111) surfaces during ReaxFF-MD simulations. (a, e) The generated  $\text{NH}_x$  ( $\text{NH}_x = \text{NH} + \text{NH}_2 + \text{NH}_3$ ), (b, f)  $\text{NH}$ , (c, g)  $\text{NH}_2$  and  $\text{NH}_3$  molecules, and (d, h) the dissociated  $\text{H}_2$  molecules on Fe surfaces. Here, several strains were applied: 0% (dark-gray), 3% (dark-blue), and 5% (orange). (For interpretation of the references to color in this figure legend, the reader is referred to the Web version of this article.)



**Fig. 4** – (a–c) The average energies of (a) Fe, (b) N, and (c) H atoms for the Fe(110) and Fe(111) catalyst systems, where each data point is averaged by the numbers of Fe, N, or H atoms. The dotted lines denote the point where the 5% strain is applied, indicating that the light-gray shaded areas are under strain. (d–e) The von Mises stress analyses of (d) Fe(110) and (e) Fe(111) systems during MD simulations, where the insets of (i)–(iv) depict the von Mises stresses of N atoms only. Continuous strain is applied at 2.5 ps (right) for both systems. To compare the stress changes between Fe surfaces, each atomic stress value is normalized using the maximum stress of Fe. (For interpretation of the references to color in this figure legend, the reader is referred to the Web version of this article.)

Table 1 summarizes the changes in the average von Mises stress of Fe and N with MD time. Initially ( $t = 0$  ns), Fe(111) shows a higher average von Mises stress of Fe (21.1 GPa) than Fe(110) (19.4 GPa) because Fe(111) is a more activated surface. When strain is applied to the Fe(110) surface, the average von Mises stress of Fe increases by 10.5% compared to the initial value. The average von Mises stress of N significantly increases by 31.8% over the initial value, which is approximately twice the increment for the system without external strain. These results clearly show that the external strain can significantly activate Fe and N atoms on Fe(110), particularly N atoms. For Fe(111), the average von Mises stress of N increases by 26.3% after 1 ns even under no strain. However, although the strain is applied to Fe(111), the strain effect is not significant, which is similar to the results shown in Figs. 1 and 3. At 1 ns, the average von Mises stresses of N on both surfaces under strain are similar (41.0 GPa vs. 40.6 GPa), resulting from the significant increase in the von Mises stress

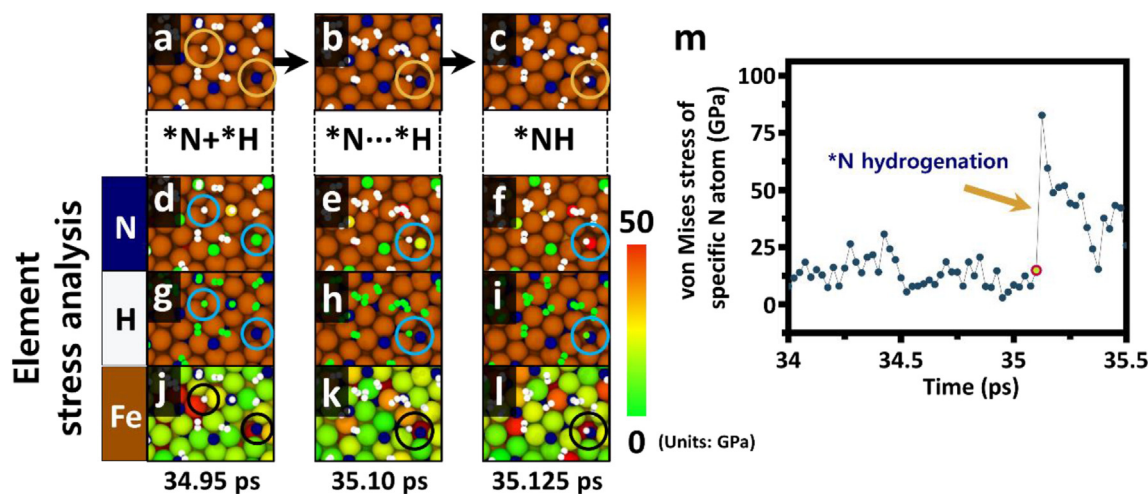
for the Fe(110) system. In Table 1, we also confirm the correlation between the change in von Mises stress and the catalyst activity for  $\text{NH}_x$  ( $x = 1-3$ ) generation. In other words, when no strain is applied, Fe(111) generates more  $\text{NH}_x$ , which correlates with the fact that Fe(111) has a higher von Mises stress than Fe(110). However, Fe(111) shows a negligible strain effect, while the von Mises stress of Fe and N atoms on Fe(110) significantly increases by the external strain, and then the highly activated Fe and N atoms promote  $\text{NH}_x$  generation.

Fig. 5 shows the von Mises analysis of  $\text{*NH}$  formation from  $\text{*N}$ . The stress value of  $\text{*N}$  slightly fluctuates over time; however, the stress is significantly increased when forming  $\text{*NH}$  (Fig. 5m). Similar behavior is also observed during the formation of  $\text{*NH}_2$  from  $\text{*NH}$  in Fig. S14. These clearly show the correlation between the von Mises stresses and the chemical reactivities of atoms. This phenomenon is observed for all systems regardless of strain, but the  $\text{NH}_3$  formation rate is

**Table 1** – Changes in the average von Mises stress of Fe and N atoms and the generated NH<sub>x</sub> on Fe(110) and Fe(111) catalysts with and without strain compared to the initial values at 0 ns.

	Time (ns)	Changes of the average von Mises stress (%)				Generated NH <sub>x</sub> (μmol/m <sup>2</sup> )	
		Fe		N		No strain	5%
		No strain	5%	No strain	5%		
Fe(110)	0	19.4 <sup>a</sup>	–	31.1 <sup>a</sup>	–	0	0
	0.25	+1.4	+7.4	+4.6	+15.1	1.4	2.7
	0.5	+2.1	+8.7	+9.2	+23.0	2.6	4.1
	0.75	+2.5	+10.1	+13.0	+28.0	3.3	5.6
	1	+3.1	+10.5	+16.8	+31.8	4.1	6.6
Fe(111)	0	21.1 <sup>a</sup>	–	31.1 <sup>a</sup>	–	0	0
	0.25	+0.4	+1.5	+7.9	+10.1	1.6	1.3
	0.5	+1.7	+2.9	+16.3	+19.6	3.4	3.1
	0.75	+1.4	+3.3	+21.7	+25.6	4.6	4.2
	1	+1.7	+3.7	+26.3	+30.4	6.0	5.5

<sup>a</sup> The initial von Mises stresses are in GPa.



**Fig. 5** – The von Mises stress analysis during the hydrogenation reaction of \*N (\*N + \*H → \*NH) on the Fe(110) surface. (a–c) MD snapshots before hydrogenation (t = 34.95 ps), diffusion of \*H (t = 35.10 ps), and \*NH formation (t = 35.125 ps). Here, the color code for atoms is Fe = brown, N = navy, and H = white. (d–l) The von Mises stress distributions of N, H, and Fe atoms at each MD time step. (m) The von Mises stress of \*N interacting with \*H. A red circle point at 35.10 ps indicates a step where the hydrogenation starts. (For interpretation of the references to color in this figure legend, the reader is referred to the Web version of this article.)

much faster under strain. The difference in the reaction rates results from the energy gain supplied by strain. When strain is applied, more energy is transferred to the Fe catalysts and surface-adsorbed atoms, increasing their reactivities.

#### Mechanochemical hydrogenation mechanism

According to our ReaxFF-MD simulations, the hydrogenation of \*N occurs in two ways: (1) the \*H dissociated on Fe surfaces is diffused to \*N to form \*NH (\*N + \*H → \*NH + \*) (Fig. 6a, Scheme 1), and (2) a H<sub>2</sub> molecule directly interacts with \*N (\*N + H<sub>2</sub> + \* → \*NH + \*H) (Fig. 6a, Scheme 2). Here, we focus on the hydrogenation reaction of \*N because it is the rate-determining step in mechanochemical NH<sub>3</sub> synthesis [12]. Our MD simulations reveal that Scheme 2 is preferentially

observed for \*NH formation. Although the first path has been reported in several studies [57,58], the second path has not yet been reported. Thus, NEB calculations are considered to compare the energetics of the two paths (Fig. 6b). The NEB results show that Scheme 2 is kinetically and thermodynamically more favorable than Scheme 1, in which the energy barrier for Scheme 2 (0.5 eV) is lower than that of Scheme 1 (1.5 eV). Moreover, the reaction is exothermic in Scheme 2, while Scheme 1 is energetically slightly uphill. These results clearly support our ReaxFF-MD simulations. Here, we conclude that \*NH formation in the mechanochemical process occurs via both Schemes 1 and 2, although Scheme 2 is preferential. Moreover, we also analyzed the von Mises stresses of atoms during \*NH formation via Scheme 2 (Fig. S15) and found that mechanical strain readily promotes \*NH formation via Scheme

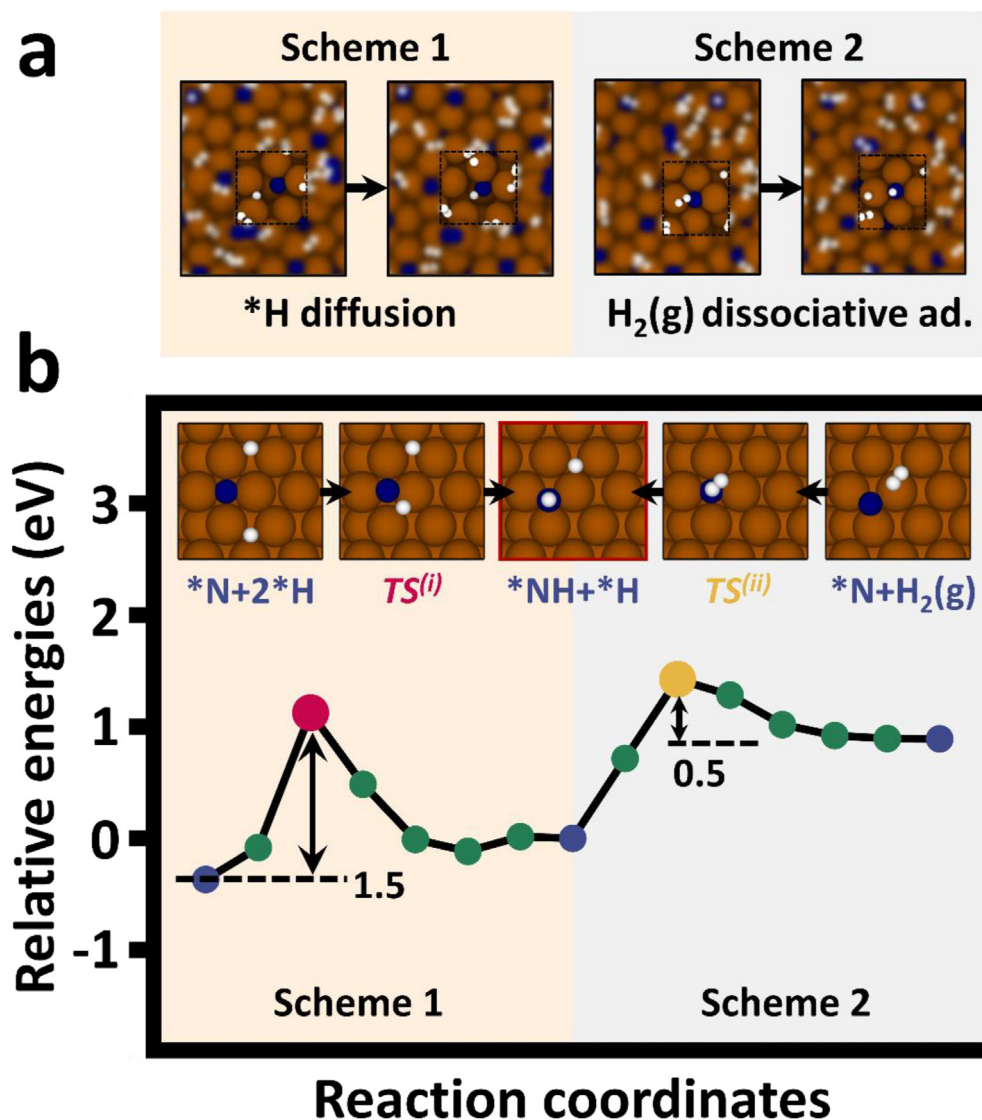


**Fig. 6 – (a) Two hydrogenation paths for \*NH formation on Fe catalysts. Scheme 1 indicates  $*N + *H \rightarrow *NH + *$ , and Scheme 2 indicates  $*N + H_2 + * \rightarrow *NH + *H$ . (b) NEB results for Scheme 1 and Scheme 2 obtained by DFT calculations. (For interpretation of the references to color in this figure legend, the reader is referred to the Web version of this article.)**

2, which is similar to the results shown in Fig. 5. For the formation of  $*NH_2$  and  $*NH_3$  in our MD simulations, a similar mechanism to Scheme 1 based on the surface diffusion of  $*H$  is dominant, as reported in the literature [57,59].

In this work, we simulated the two-step process for  $NH_3$  synthesis consisting of  $N_2$  dissociation and then hydrogenation reactions similar to the previous experiment [12]. In a similar way, we additionally simulated one-step process reactions for  $NH_3$  synthesis in which  $H_2$  and  $N_2$  molecules can interact with Fe surfaces at the same time (Fig. S16). It reveals that the mechanical strain enhances catalytic performance irrespective of the one-/two-step reactions. The one step reaction leads to two times more  $NH_x$  products under strain than the one without strain. Yet, the two-step reaction (Fig. 3) would produce more  $NH_x$  products compared to the one-step reaction after 1.5 ns of MD simulations.

## Conclusion

The mechanochemical way for  $NH_3$  synthesis on Fe catalysts has been explored to clarify the atomistic origin by ReaxFF-MD simulations, in which we investigate the effects of the applied strain on Fe surfaces on  $NH_3$  synthesis. From the von Mises stress analysis, the mechanical stress induced by the exerted strain readily activates the  $NH_x$  ( $x = 1-3$ ) formation reactions. In particular, the strain effect is much more pronounced on Fe(110) than on Fe(111). Although Fe(111) is more active for  $NH_3$  formation than Fe(110) when no strain is applied, the applied strain can significantly increase the activity of Fe(110) as much as Fe(111). Considering that Fe(110) is the thermodynamically most favorable surface, the mechanochemical process can readily enhance the activity of Fe catalysts for  $NH_3$  synthesis.

On the other hand, in the actual experiment, various defects on Fe surfaces can be generated during the ball-milling process and are highly activated for N<sub>2</sub> dissociation [12,60]. Although this work does not consider defects, we can readily conclude that mechanical stress activates Fe surfaces for NH<sub>3</sub> formation, particularly Fe(110), even without the help of defects.

### Declaration of competing interest

The authors declare that they have no known competing financial interests or personal relationships that could have appeared to influence the work reported in this paper.

### Acknowledgement

This work was supported by the Creative Materials Discovery Program through the National Research Foundation of Korea (2016M3D1A1021141) and the National Center for Materials Research Data (NCMRD) through the National Research Foundation of Korea funded by the Ministry of Science and ICT (2021M3A7C2089739).

### Appendix A. Supplementary data

Supplementary data to this article can be found online at <https://doi.org/10.1016/j.ijhydene.2022.10.193>.

### REFERENCES

- Chen JG, Crooks RM, Seefeldt LC, Bren KL, Bullock RM, Darensbourg MY, Holland PL, Hoffman B, Janik MJ, Jones AK, Kanatzidis MG, King P, Lancaster KM, Lyman SV, Pfromm P, Schneider WF, Schrock RR. Beyond fossil fuel-driven nitrogen transformations. *Science* 2018;360:1–7.
- Aziz M, Putranto A, Biddinika MK, Wijayanta AT. Energy-saving combination of N<sub>2</sub> production, NH<sub>3</sub> synthesis, and power generation. *Int J Hydrogen Energy* 2017;42:27174–83.
- Faria JA. Renaissance of ammonia synthesis for sustainable production of energy and fertilizers. *Curr Opin Green Sustain Chem* 2021;29:100466.
- Rouwenhorst KHR, Van der Ham AGJ, Lefferts L. Beyond Haber-Bosch: the renaissance of the claud process. *Int J Hydrogen Energy* 2021;46:21566–79.
- Smith C, Hill AK, Torrente-Murciano L. Current and future role of Haber-Bosch ammonia in a carbon-free energy landscape. *Energy Environ Sci* 2020;13:331–44.
- Suryanto BHR, Du H-L, Wang D, Chen J, Simonov AN, MacFarlane DR. Challenges and prospects in the catalysis of electroreduction of nitrogen to ammonia. *Nat Catal* 2019;2:290–6.
- MacFarlane DR, Cherepanov PV, Choi J, Suryanto BHR, Hodgetts RY, Bakker JM, Vallana FMF, Simonov AN. A roadmap to the ammonia economy. *Joule* 2020;4:1186–205.
- Guo J, Chen P. Catalyst: NH<sub>3</sub> as an energy carrier. *Chem* 2017;3:709–14.
- Kojima Y, Yamaguchi M. Ammonia as a hydrogen energy carrier. *Int J Hydrogen Energy* 2022;47:22832–9.
- Banisalman MJ, Kim M-C, Han SS. Origin of enhanced ammonia synthesis on Ru–Co catalysts unraveled by density functional theory. *ACS Catal* 2022;12:1090–7.
- Kim M-C, Nam H, Choi J, Kim HS, Lee HW, Kim D, Kong J, Han SS, Lee SY, Park HS. Hydrogen bonding-mediated enhancement of bioinspired electrochemical nitrogen reduction on Cu<sub>2-x</sub>S catalysts. *ACS Catal* 2020;10:10577–84.
- Han G-F, Li F, Chen Z-W, Coppex C, Kim S-J, Noh H-J, Fu Z, Lu Y, Singh CV, Siahrostami S, Jiang Q, Baek J-B. Mechanochemistry for ammonia synthesis under mild conditions. *Nat Nanotechnol* 2021;16:325–30.
- Gong Y, Wu J, Kitano M, Wang J, Ye T-N, Li J, Kobayashi Y, Kishida K, Abe H, Niwa Y, Yang H, Tada T, Hosono H. Ternary intermetallic LaCoSi as a catalyst for N<sub>2</sub> activation. *Nat Catal* 2018;1:178–85.
- Shipman MA, Symes MD. Recent progress towards the electrosynthesis of ammonia from sustainable resources. *Catal Today* 2017;286:57–68.
- James SL, Adams CJ, Bolm C, Braga D, Collier P, Friščić T, Grepioni F, Harris KDM, Hyett G, Jones W, Krebs A, Mack J, Maini L, Orpen AG, Parkin IP, Shearouse WC, Steed JW, Waddell I, D. C. Mechanochemistry: opportunities for new and cleaner synthesis. *Chem Soc Rev* 2012;41:413–47.
- Merrill PB, Madix RJ. Hydrogen bonding on iron: correlation of adsorption and desorption states on Fe(100) and perturbation of the Fe-H bond with coadsorbed CO. *Surf Sci* 1996;347:249–64.
- Wang T, Wang S, Luo Q, Li Y-W, Wang J, Beller M, Jiao H. Hydrogen adsorption structures and energetics on iron surfaces at high coverage. *J Phys Chem C* 2014;118:4181–8.
- Medford AJ, Vojvodica A, Hummelshøj JS, Voss J, Abild-Pedersen F, Studt F, Bligaard T, Nilsson A, Nørskov JK. From the Sabatier principle to a predictive theory of transition-metal heterogeneous catalysis. *J Catal* 2015;328:36–42.
- Wang Q, Guo J, Chen P. Recent progress towards mild-condition ammonia synthesis. *J Energy Chem* 2019;36:25–36.
- Juangsang FB, Irhamna AR, Aziz M. Production of ammonia as potential hydrogen carrier: review on thermochemical and electrochemical processes. *Int J Hydrogen Energy* 2021;46:14455–77.
- Senftle TP, Hong S, Islam MM, Kylasa SB, Zheng Y, Shin YK, Junkermeier C, Engel-Herbert R, Janik MJ, Aktulga HM, Verstraelen T, Grama A, van Duin ACT. The ReaxFF reactive force-field: development, applications and future directions. *Npj Comput. Mater.* 2016;2(15011):1–14.
- van Duin ACT, Dasgupta S, Lorant F, Goddard III WA. ReaxFF: A reactive force field for hydrocarbons. *J Phys Chem A* 2001;105:9396–409.
- Yeo BC, Jung H, Lee HW, Yun K-S, Kim H, Lee K-R, Han SS. Atomistic simulation protocol for improved design of Si-O-C hybrid nanostructures as Li-ion battery anodes: ReaxFF reactive force field. *J Phys Chem C* 2017;121:23268–75.
- Bedrov D, Smith GD, van Duin ACT. Reactions of singly-reduced ethylene carbonate in lithium battery electrolytes: a molecular dynamics simulation study using the ReaxFF. *J Phys Chem A* 2012;116:2978–85.
- Lee JS, Kaufman-Osborn T, Melitz W, Lee S, Delabie A, Sioncke S, Caymax M, Pourtois G, Kummel AC. Atomic imaging of nucleation of trimethylaluminum on clean and H<sub>2</sub>O functionalized Ge(100) surfaces. *J Chem Phys* 2011;135:054705.
- Chenoweth K, van Duin ACT, Goddard III WA. ReaxFF reactive force field for molecular dynamics simulations of hydrocarbon oxidation. *J Phys Chem A* 2008;112:1040–53.
- Qian H-J, van Duin ACT, Morokuma K, Irle S. Reactive molecular dynamics simulation of fullerene combustion synthesis: ReaxFF vs DFTB potentials. *J Chem Theor Comput* 2011;7:2040–8.

- [28] Cheng T, Jaramillo-Botero A, Goddard III WA, Sun H. Adaptive accelerated ReaxFF reactive dynamics with validation from simulating hydrogen combustion. *J Am Chem Soc* 2014;136:9434–42.
- [29] Agrawalla S, van Duin ACT. Development and application of a ReaxFF reactive force field for hydrogen combustion. *J Phys Chem A* 2011;115:960–72.
- [30] Monti S, Corozzi A, Frstrup P, Joshi KL, Shin YK, Oelschlaeger P, van Duin ACT, Barone V. Exploring the conformational and reactive dynamics of biomolecules in solution using an extended version of the Glycine reactive force field. *Phys Chem Chem Phys* 2013;15:15062–77.
- [31] Banisalman MJ, Lee HW, Koh H, Han SS. Atomistic insights into H<sub>2</sub>O<sub>2</sub> direct synthesis of Ni–Pt nanoparticle catalysts under water solvents by reactive molecular dynamics simulations. *ACS Appl. Mater* 2021;13(15):17577–85.
- [32] Chenoweth K, van Duin ACT, Goddard III WA. The ReaxFF Monte Carlo reactive dynamics method for predicting atomistic structures of disordered ceramics: Application to the Mo<sub>3</sub>VO<sub>x</sub> Catalyst. *Angew Chem Int Ed* 2009;48:7630–4.
- [33] Han Y, Ma T, Chen F, Li W, Zhang J. Supercritical water gasification of naphthalene over iron oxide catalyst: a ReaxFF molecular dynamics study. *Int J Hydrogen Energy* 2019;44:30486–98.
- [34] Kim S-Y, Lee HW, Pai SJ, Han SS. Activity, selectivity, and durability of ruthenium nanoparticle catalysts for ammonia synthesis by reactive molecular dynamics simulation: the size effect. *ACS Appl Mater Interfaces* 2018;10:26188–94.
- [35] Islam MM, Zou C, van Duin ACT, Raman S. Interactions of hydrogen with the iron and iron carbide interfaces: a ReaxFF molecular dynamics study. *Phys Chem Chem Phys* 2016;18:761–71.
- [36] van Duin ACT, Baas JMA, van de Graaf B. Delft molecular mechanics: a new approach to hydrocarbon force fields. Inclusion of a geometry-dependent charge calculation. *J Chem Soc, Faraday Trans* 1994;90:2881–95.
- [37] Kresse G, Furthmüller J. Efficiency of ab-initio total energy calculations for metals and semiconductors using a plane-wave basis set. *Comput Mater Sci* 1996;6:15–50.
- [38] Hammer B, Hansen LB, Nørskov JK. Improved adsorption energetics within density-functional theory using revised Perdew-Burke-Ernzerh of functionals. *Phys Rev B* 1999;59:7413–21.
- [39] Kresse G, Joubert D. From ultrasoft pseudopotentials to the projector augmented-wave method. *Phys Rev B* 1999;59:1758–75.
- [40] Sheppard D, Terrell R, Henkelman G. Optimization methods for finding minimum energy paths. *J Chem Phys* 2008;128:134106.
- [41] Plimpton S. Fast parallel algorithms for short-range molecular dynamics. *J Comput Phys* 1995;117:1–19.
- [42] Aktulga HM, Fogarty JC, Pandit SA, Grama AY. Parallel reactive molecular dynamics: Numerical Methods and Algorithmic Techniques. *Parallel Comput.* 2012;38:245–59.
- [43] Strongin DR, Carrazza J, Bare SR, Somorjai GA. The importance of C7 sites and surface roughness in the ammonia synthesis reaction over iron. *J Catal* 1987;103:213–5.
- [44] Chen X, Kawai K, Zhang H, Fukuzawa K, Koga N, Itoh S, Azuma N. ReaxFF reactive molecular dynamics simulations of mechano-chemical decomposition of perfluoropolyether lubricants in heat-assisted magnetic recording. *J Phys Chem C* 2020;124:22496–505.
- [45] Rappe AK, Casewit CJ, Colwell KS, Goddard III WA, Skiff WM. UFF, a full periodic table force field for molecular mechanics and molecular dynamics simulations. *J Am Chem Soc* 1992;114(25):10024–35.
- [46] Dudarev SL, Arakawa K, Yi X, Yao Z, Jenkins ML, Gilbert MR, Derlet PM. Spatial ordering of nano-dislocation loops in ion-irradiated materials. *J Nucl Mater* 2014;455:16–20.
- [47] Emmett PH, Brunauer S. The adsorption of nitrogen by iron synthetic ammonia catalysts. *J Am Chem Soc* 1934;56:35.
- [48] Ertl G, Lee SB, Weiss M. Adsorption of nitrogen on potassium promoted Fe(111) and (100). *Surfaces Surf. Sci.* 1982;114:527–45.
- [49] Bozso F, Ertl G, Grunze M, Weiss M. Interaction of nitrogen with iron surfaces: I. Fe (100) and Fe (111). *J Catal* 1977;49:18–41.
- [50] Bozso F, Ertl G, Weiss M. Interaction of nitrogen with iron surfaces: II. Fe(110). *J Catal* 1977;50:519–29.
- [51] Spencer ND, Schoonmaker RC, Somorjai GA. Iron single crystals as ammonia synthesis catalysts: effect of surface structure on catalyst activity. *J Catal* 1982;74:129–35.
- [52] Logadottir A, Nørskov JK. The effect of strain for N<sub>2</sub> dissociation on Fe surfaces. *Surf Sci* 2001;489:135–43.
- [53] Yeo SC, Han SS, Lee HM. Adsorption, dissociation, penetration, and diffusion of N<sub>2</sub> on and in bcc Fe: first-principles calculations. *Phys Chem Chem Phys* 2013;15:5186–92.
- [54] Goikoetxea I, Alducin M, Muiño RD, Juaristi JI. Dissociative and non-dissociative adsorption dynamics of N<sub>2</sub> on Fe(110). *Phys Chem Chem Phys* 2012;14:7471–80.
- [55] Xu L, Kirvassilis D, Bai Y, Mavrikakis M. Atomic and molecular adsorption on Fe(110). *Surf Sci* 2018;667:54–65.
- [56] Duan X, Jia J, Qiana G, Fan C, Zhu Y, Zhou X, Chen D, Yuan W. Ammonia decomposition on Fe (1 1 0), Co (1 1 1) and Ni (1 1 1) surfaces: a density functional theory study. *J Mol Catal A Chem* 2012;357:81–6.
- [57] Qian J, An Q, Fortunelli A, Nielsen RJ, Goddard III WA. Reaction mechanism and kinetics for ammonia synthesis on the Fe(111) surface. *J Am Chem Soc* 2018;140:6288–97.
- [58] Armenise S, García-Bordejé E, Valverde JL, Romeo E, Monzón A. A Langmuir–Hinshelwood approach to the kinetic modelling of catalytic ammonia decomposition in an integral reactor. *Phys Chem Chem Phys* 2013;15:12104–17.
- [59] Hellmana A, Honkalab K, Remediakis IN, Logadottir, Á.; Carlsson, A.; dahl, S.; Christensen, C. H.; Nørskov, J. K. Ammonia synthesis and decomposition on a Ru-based catalyst modeled by first-principles. *Surf Sci* 2009;603:1731–9.
- [60] Honkala K, Hellman A, Remediakis IN, Logadottir A, Carlsson A, Dahl S, Christensen CH, Nørskov JK. Ammonia synthesis from first-principles calculations. *Science* 2005;307:555–8.